Published in final edited form as:
Anal Chem. 2013 September 17; 85(18): . doi:10.1021/ac400062v.

Real Time Analysis of Binding between Rituximab (anti-CD20 antibody) and B Lymphoma Cells

Liang Tan[†,‡], **Peiling Lin**[†], **Mohammad M. Chisti**[§], **Abdul Rehman**[†], and **Xiangqun Zeng**[†,*]

[†]Chemistry Department, Oakland University, Rochester, Michigan 48309, United States

[‡]Key Laboratory of Chemical Biology and Traditional Chinese Medicine Research (Ministry of Education of China), College of Chemistry and Chemical Engineering, Hunan Normal University, Changsha, 410081, PR China

[§]Department of Hematology and Oncology, William Beaumont Hospital, Royal Oak, Michigan 48073, United States

Abstract

CD20, expressed on greater than 90% of B-lymphocytic lymphomas, is an attractive target for antibody therapy. Rituximab is a chimeric murine/human-engineered monoclonal antibody and can selectively deplete CD20-expressing cells in peripheral blood and lymphoid tissues. The immobilization of B-lymphoblast-like Burkitt's lymphoma Raji cells on the quartz crystal microbalance (QCM) gold electrode surface using RGD tripeptide was electrochemically confirmed. The real-time processes of attachment of Raji cells on the gold electrode and the subsequent binding of Rituximab to the cells were studied using QCM biosensor. The interaction between Rituximab and Raji cells led to the increased resonant frequency shifts (Δf_0) in the studied antibody concentration range from 5 to 250 μg mL^{-1} following the Langmuir adsorption model. From these observations, the apparent binding constant between a single-layer of Rituximab and Raji cells was calculated to be 1.6×10^6 M^{-1}. Control experiments using other therapeutic antibodies (i.e., Trastuzumab and Bevacizumab) and different cells (i.e., T cells and endothelial cells) proved the specific interaction between Rituximab and B cells. The effects of Ca^{2+} and Mn^{2+} ions on the Rituximab-Raji cell interaction were also studied providing the enhanced QCM signals, in particular, further indicating that CD20 is a calcium ion channel that can transport these metal ions into the cells and accelerate the cell lysis induced by Rituximab. Thus the real time capability of QCM and its simplicity of operation are highly suitable for multipurpose studies on living cells including cell-immobilization, cytotoxicity of drugs, and the cell action mechanisms.

Keywords

Rituximab; CD20; Raji cells; specific binding; calcium ion channel; QCM

INTRODUCTION

The characterization of the property of surface antigen of a cancer cell is essential in the understanding of the disease and in the development of targeted therapy. CD20 is a 35–37

*Corresponding Author. zeng@oakland.edu.

ASSOCIATED CONTENT

Supporting Information. Figures S1–S6 are provided as supporting information. This material is available free of charge via the Internet at http://pubs.acs.org.

kDa non-glycosylated tetra-spanning membrane protein expressed by B lymphocytes in early stages of differentiation and by most B cell lymphomas.[1] It can be found on pre-B cells in bone marrow and on immature and mature B cells in blood and lymphoid tissues.[2] The function of CD20 is not fully understood, although this protein is thought to play a role in B-cell activation, regulation of cell growth, and trans-membrane calcium flux.[3] CD20 has been regarded as an attractive target for antibody therapy for the treatment of non-Hodgkin's lymphoma. Moreover, targeting CD20 on B lymphocytes has been shown to be a relatively safe therapy because CD20 antigen is absent on stem cells.[4] The chimeric murine/human-engineered monoclonal anti-CD20 antibody, Rituximab, is a pivotal drug approved for almost all types of lymphomas[5,6] and some autoimmune diseases.[7,8] Although Rituximab has achieved unprecedented success in clinics, exhibiting significant anti-tumor activity and promoting the survival rates of lymphoma patients, many questions remained unanswered regarding its therapeutic effect which is likely related to the binding properties of Rituximab and the CD20 on the cell surface. For instance, it is unclear why 50% of the patients with B-cell non-Hodgkin's lymphoma do not respond.[4,9] Resistance to further Rituximab therapy may be found in a majority of responsive patients as well.[10] Several novel second-generation monoclonal antibodies targeting CD20 antigen have been developed to achieve improved response rates as compared to Rituximab, but that may expose the patients to more toxic, co-administered therapeutic agents, thus marking the need of potency enhancement strategies for the same drug.[11]

CD20 expression in lymphomas is heterogeneous. Studies have already shown that reduced CD20 expression is associated with inferior survival and different behavior of lymphomas including Diffuse Large B Cell Lymphoma (DLBCL), Chronic Lymphocytic Leukemia (CLL) and Hodgkin's Lymphomas.[12–14] Patients who have reduced CD20 expression on their biopsies taken at diagnosis have a markedly inferior overall survival after treatment with chemotherapy with or without Rituximab. Moreover, quantitative measurements of fluorescence intensity using micro-bead standards would be considered as the "gold standard" in determining the number of antigens on specific cell populations of interest,[15] but CD20 antigen density measurement with flow cytometry (FCM) is also heterogeneous.[12] Thus, in order to identify factors that can accurately predict clinical responsiveness of anti-CD20 antibody, to develop ways to augment anti-CD20 antibody activity, and even to create novel and more potent anti-CD20 antibodies, it is important to develop a biosensor that can quantify the expression of CD20 antigen on cancer B cells and study the in situ binding phenomena as a function of time, between anti-CD20 antibody, such as Rituximab and CD20-overexpressing cancer cells.

Quartz crystal microbalance (QCM)[16,17] has long been recognized as a standard non-invasive tool to detect such bio-molecular interactions (e.g., antigen or peptide/antibody interactions) in real-time without using labels (e.g., fluorescent dye or enzyme-conjugated secondary antibodies). QCM not only can provide information about mass loading but also can reveal the physicochemical properties including elastic moduli, density, and viscosity near the electrode surface, thus indicating even the slight morphological changes in the immobilized species (e.g., cell expansion or lysis). The most common quantification principles for the QCM technique are based either on its mass-frequency correlation described by Sauerbrey equation[18] or its viscodensity effect equations described by Kanazawa and Gordon[19] as well as Martin and Granstaff et al.[20,21] Based on these principles, we have originated many different strategies to develop piezoimmunosensor assays.[22–28] This work is the first demonstration of this strategy, where the binding reaction between the cancerous B cell surface-antigens and antibody-drugs has been studied using anti-CD20 antibody Rituximab as an example. In order to achieve this goal, we designed a biointerface for quantitative immobilization of cancerous B cells. Rather than protein receptor, arginine-glycine-aspartic acid amino acids (RGD) tripeptide was immobilized on

the gold surface. The RGD tripeptide is the recognized minimal adhesion domain of most extracellular matrix proteins (ECM) which binds selectively with integrin receptors in all the cellular adhesion phenomena.[29,30] It was used as an anchor to quantitatively capture cells for their immobilization in the present work. Cyclic voltammetry (CV) and electrochemical impedance (EI) measurements were employed to investigate the interfacial properties of the cell modified electrode surfaces. With this experimental design, the real-time binding of Rituximab and control therapeutic monoclonal antibodies including Trastuzumab and Bevacizumab to B cells and control cells including suspension cells and attachment cells were characterized using QCM transducer. However, as the setup is much like the *in vivo* representing endogenous conditions and involving multiple binding factors, the calculated constant for this binding process between Rituximab and B lymphoma cells by taking advantage of the high sensitivity of QCM can be termed as the apparent binding constant.[31] Furthermore, the intake of Ca^{2+} and Mn^{2+} ions by cells and their effect on the cell lysis induced by Rituximab were studied which provides some information of CD20 on cell membranes as a calcium ion channel. In comparison with widely used bioassay methods such as flow cytometry, the biosensor using QCM technique shown here allows us to quantify the binding of anti-CD20 antibody with the cell surface CD20 antigen real time. Application of this new biosensor technology will enable us to understand surface antigen expression of tumor cells, evaluate their density, and characterize the role of different ion channels in these malignancies in context of therapeutical drug treatments such as with Rituximab and Ofatumomab.

EXPERIMENTAL SECTION

Materials and apparatus

The therapeutic monoclonal antibodies (mAbs) including Rituxan (Rituximab), Herceptin (Trastuzumab) and Avastin (Bevacizumab) were provided by Beaumont Hospital, Royal Oak, Michigan. HEPES buffered saline (HBS, pH 7.4) was obtained from Biacore Life Sciences (Sweden) and used in cell-based experiments. Phosphate-buffered saline (PBS, pH 7.4) was purchased from Invitrogen and employed in the electrochemical measurements. A 0.25 mol L^{-1} L-cysteine (Cys, Sigma) solution was prepared with 0.1 mol L^{-1} hydrochloric acid. A 1 mg mL^{-1} arginine-glycine-aspartic acid (RGD) tripeptide (Sigma) solution was prepared with biological grade water (resistance greater than 18 MΩ, and further filtered with a 0.2 μm filter). Other chemicals were of analytical reagent grade.

The gold QCM electrode consists a thin AT-cut quartz crystal wafer with one gold electrode on each side (10 MHz, non-polished with ~1000 Å gold, geometric area is 0.22 cm^2, International Crystal Company). The Au QCM electrode was mounted on the side of a Kel-F chamber. RQCM instrument (Maxtek Inc., USA) was used to simultaneous recording of resonant frequency (f_0) and motional resistance (R_1) of the QCM electrodes. A Lawson EMF-16 precision electrochemistry EMF interface instrument (Malvern, PA, USA) was used to monitor equilibrium potential change in real time. Cyclic voltammetry (CV) and electrochemical impedance spectroscopy (EIS) experiments were performed with a potentiostat/galvanostat (EG&G Par model 2263) by using a three-electrode electrolytic cell. QCM electrode acted as the working electrode. A Ag/AgCl reference electrode (saturated KCl) served as the reference electrode. A platinum wire served as the counter electrode. The cell-modality observation was performed using an inverted optical microscope (Nikon TMS-F, Japan) with a digital camera (SPOT, 1600×1200 pixels, Diagnostic Instrument Inc. USA).

RGD tripeptide immobilization

The assembly process of RGD tripeptide is shown in Scheme 1. To remove possible contamination, the QCM electrode surface was cleaned with Piranha solution (30% H_2O_2:

H_2SO_4 3:7). Then the surface was thoroughly rinsed with water and blown dry with a stream of nitrogen gas. The freshly cleaned QCM electrode was immersed into cysteine solution overnight. Subsequently, the Cys-modified QCM electrode was immersed in 5% glutaraldehyde (GA) aqueous solution for 0.5 h. Finally, 20 μl of 1 mg ml^{-1} RGD aqueous solution was added on the dry GA/Cys-modified gold surface for one hour. The electrode was gently washed with the biological grade water and then nitrogen-dried after each assembly process.

Cell culture and measurement procedures

Burkitt's lymphoma Raji cells, acute lymphoblastic leukemia CCRF-CEM cells and vascular endothelium HUVEC-C cells were obtained from American Type Culture Collection (ATCC). They were cultured using RPMI-1640 growth medium (Gibco) supplemented with 10% fetal calf serum (Gibco) and F-12K medium (ATCC) supplemented with 0.1 mg ml^{-1} heparin (Sigma), 0.03 mg ml^{-1} endothelial cell growth supplement (ECGS, Sigma), and 10% fetal bovine serum (Gibco) respectively, in an incubator (5% CO_2, 37 °C).

The RGD-assembled QCM electrode was mounted on the side of the measuring chamber containing 1.9 mL HBS. This set-up ensures the binding of the analyte with the immobilized cells on the QCM electrode. The QCM signals were obtained under stirring condition. The density of cells was determined with a hemacytometer. After the concentration of cells reached 1×10^6 cells mL^{-1}, they were collected from the medium by centrifugation at 1500 g for 5 min, and washed with HBS for three times. Then 100 μL of the cell-suspending solution was added evenly into the measuring chamber. The Δf_0 and ΔR_1 responses were simultaneously monitored up to 20 hours. The therapeutic mAbs were added at two hour after the addition of cells.

RESULTS AND DISCUSSION

Characterization of the immobilization of cell on the gold electrode surface

It is well known that Raji cells belong to suspension cells. Their immobilization on the electrode surface is not easily achievable. So RGD tripeptide was employed to capture Raji cells. The cell immobilization was characterized by electrochemical methods. Figure 1 exhibits the cyclic voltammograms and electrochemical impedance spectroscopy of modified QCM electrodes before and after each step of modifications. The immobilization of RGD tripeptide results in the decrease of the peak currents of ferri-/ferrocyanide probe (shown in CV) and increase of the electron transfer resistance of ferri-/ferrocyanide probe (shown in the Nyquist impedance plot). Both results suggest that the modified thin film efficiently blocked the electron transfers of ferri-/ferrocyanide probe. The above electrochemical parameters were changed to a greater extent with the introduction of Raji cells, proving the cell was captured by the RGD modified electrode. In addition, one can find that the changes of currents and electron transfer resistances derived from the cell capture were smaller than those induced by the immunoreactions described in our former work.[22,23] In general, suspension cells present spherical shape and their size is far smaller than that of adhesive cells. So there were still some spaces for the entering of ferri-/ferrocyanide probe even if the suspension cells were immobilized in a close packing manner on the electrode surface. As a result, the changing extent of the electrochemical parameters was not large. The similar CV and EIS experimental results induced by the capture of leukemia K562 cells, a kind of suspension cells, can be found in the reported researches.[32–34] It is interesting to be found that the peak currents and the electron transfer resistance were increased and decreased, respectively, after the cell-captured electrode suffered the 16-hour treatment of Rituximab. It suggests that Rituximab induced the change of Raji cell properties, which should be the cell death, resulting in the detachment of the

broken cells from the electrode and the increased opportunity of the electron transfers of ferri-/ferrocyanide probe on the electrode surface.

Figure S1A shows an obvious oxidative peak at about 0.82 V appeared (curve c) on the Raji cell modified electrode in comparison with the bare Au and the RGD modified electrodes. Similar irreversible voltammetric responses were observed for different cells at electrodes by other researchers.[35,36] The origin of this irreversible anodic peak is attributed to some of the endogenous electroactive species commonly existing in cells. One possible endogenous electroactive species rich in cytoplasm is guanine that is able to rapidly cross the cell membrane and to reach the electrode surface in the electrochemical process. The oxidation of guanine has been believed to involve the conversion of guanine to 8-oxo-guanine.[37] The anodic peak at about 0.8 V to the oxidation of the endogenous electroactive guanine in cells was verified by Ju's group using liquid chromatography-mass spectrometry.[38] We also observed that the oxidative peak at 0.82 V decreased after the cell-captured electrode suffered the treatment of Rituximab (curve d in Figure S1A) and the amount of decreased current signal was quantitatively correlated with the increase of Rituximab concentration (Figure S1B). Rituximab can induce target cell lysis via antibody-dependent cellular cytotoxicity (ADCC), complement-dependent cytotoxicity (CDC), and programmed cell death (PCD) after its binding to CD20 on B cell surface.[39] Since our experiments were done ex situ, the reduced current signal is likely due to the release of DNA from the lysed cells to the solution so that the concentration of guanine on the electrode surface is decreased.

Figure S2 shows the real-time monitoring of the capturing of the Raji cells by the RGD peptide modified electrode using potentiometry. Potentiometry allows the measurement of the electrode potential at the interface between an electrode and a solution. Changes due to the transfer of charged species across the interface, specific adsorption of ions at the interface, and the immobilization of cells at the interface will result in a potential shift. As seen in Figure S2, the initial change of equilibrium potential indicates Raji cells were attached on RGD modified gold surface. The electrode potential decreases and reaches to a constant in two hours after the addition of cells, suggesting that most of Raji cells have been successfully immobilized in this time period.

Characterization of the selective binding of Rituximab to B cells

Sauerbrey equation[18] correlates the mass change (Δm in g) and the QCM frequency change (Δf_0 in Hz) which is valid only for a thin, rigid and uniform film on the QCM electrode surface as represented in equation 1.

$$\Delta f_0 = -\frac{2f_{0g}^2}{(\rho_q \mu_q)^{1/2}} \frac{\Delta m}{A} \quad (1)$$

where f_{0g} is the fundamental frequency, A is a piezoelectrically active surface area, and ρ_q and μ_q are the density and shear modulus of quartz, respectively. QCM frequency response is sensitive not only to mass loading but also to changes in solution density and viscosity at the electrode solution interface. Martin et al. reported a series of equivalent circuit parameters and a modified Butterworth-Van Dyke (BVD) equivalent electrical circuit for the characterization of a QCM with simultaneous mass and liquid loading.[21] The relationship between the changes of the resonant frequency and those of motional resistance, Δf_0 and ΔR_1, due to net changes in solution density and viscosity can thus be obtained.[40]

$$\frac{\Delta f_0}{\Delta R_1} = -\frac{\sqrt{c_{66} f_{0g}}}{4\pi L_q \sqrt{f \mu_q}} \quad (2)$$

where L_q and f_{0g} are the motional inductance and resonant frequency of the crystal in air, respectively, f is the excitation frequency, μ_q is the shear modulus for AT-cut quartz (2.947×10^{10} N/m^2), c_{66}^{-} is the piezoelectrically stiffened elastic constant (2.957×10^{10} N/m^2), and f_{0g} can be approximately used in the calculation instead of f with error below ca. 0.3%. With these values being put into the equation 2, we can readily get $\Delta R_1 \approx -4\pi L_q \Delta f_0$. The frequency resistance slope $|\Delta f_0/\Delta R_1|$, thus calculated can be used as a quantitative representation of whether the changes in frequency can be assigned to the mass changes in the film or the viscosity variations at the interface. As ΔR_1 value is approximately zero for an ideal rigid film, the Δf_0 can only be assigned to mass changes. This means that the smaller the ΔR_1 is, the more rigid the thin film is, and more dominantly the response is due to mass. With ΔR_1 approaches towards larger values, the $|\Delta f_0/\Delta R_1|$ gets smaller reaching a threshold value below which the frequency response can predominantly be assigned to viscodensity fluctuations of the system. For 10 MHz crystal used in this work, the threshold value of the slope $|\Delta f_0/\Delta R_1|$ is 11.6 which reflects the contribution of density and viscosity in the measurement. Thus, if the slope is bigger than the absolute value of $|\Delta f_0/\Delta R_1|$ = 11.6 Hz Ω^{-1}, the frequency changes can be ascribed to be predominantly due to the mass effect.

The binding processes of three different mAbs to the Raji cell immobilized electrode were studied. Raji cells were firstly added onto the RGD tripeptide modified electrode. After two hours immobilization, mAbs were added into the biosensor system. The real-time Δf_0 and ΔR_1 responses are shown in Figure 2 (curve a) with the $|\Delta f_0/\Delta R_1|$ ratio calculated to be 24 Hz Ω^{-1} on average at the whole cell-capture phase (the slope of the dashed line 1 in Figure 2), bigger than the theoretical value for a net viscodensity effect of an AT-cut 10 MHz crystal, 11.6 Hz Ω^{-1}, which means that the QCM responses can mainly be attributed to the mass effect. Although, the changes of density and viscosity may be present, but above this threshold value, they are too small to contribute a significant effect. Moreover, these density-viscosity effects represent the combination of changes due to many different physiochemical parameters (e.g., slight changes in cell shape and matrix, and the consequential changes in behavior toward binding/unbinding to the surface and among themselves), so a complete resolution and its discussion is not worthwhile in the scope of their small magnitude. Thus in subsequent sections, majority of our focus will remain on the mass effects and the resulting binding parameters. It can be found that the addition of quantitative amount of Rituximab led to the further decreased Δf_0 and increased ΔR_1 responses. No significant change of frequency was observed for Trastuzumab and Bevacizumab control mAbs although the minor increase of resistance, which should be derived from the viscodensity-change of solution, could be observed. These results prove that Rituximab could selectively bind to Raji cells due to the interaction between Rituximab and CD20 on cell membranes. The $|\Delta f_0/\Delta R_1|$ ratio was calculated to be 14.8 Hz Ω^{-1} on average in the process of Rituximab-binding (the slope of the dashed line 2 in Figure 2). It was again bigger than 11.6 Hz Ω^{-1}, indicating that the mass effect still dominates the QCM frequency responses.

We performed a series of control experiments using other cells. Firstly, the binding of mAbs to T cells was characterized. Figure 3A1–A2 show the QCM responses to the attachment of Raji cells and CCRF-CEM cells, a type of T cells, on RGD modified electrode surface and the subsequent binding of Rituximab to the captured cells. It is interesting to find that the Δf_0 and ΔR_1 signal-changes induced by CCRF-CEM cell-adhesion were almost half of those observed from Raji cell-attachment. It means there were fewer integrin receptors on the CCRF-CEM cell-membranes and the capture of this T cells by RGD tripeptide was not easily achievable. To interpret the frequency shifts and the resistance changes in Figure 3, it is important to understand the difference of interaction mechanism of cells and the antibodies to the electrode surface of QCM. QCM is a surface sensitive technique using the generation of shear waves and their fluctuations caused by the immobilized materials. The

shear waves decay rapidly in liquid and gaseous environments. The range of penetration of a 5 MHz-shear wave in water is 250 nm. Thus, the extinction depth of the shear waves is much smaller than the cell size. Thus for the cellular interaction events, the whole ensemble of cell and its microenvironment is the response element. Contrarily, the direct adsorption of antibodies on Au QCM electrode may behave more like a rigid film, due to their existence inside the extinction boundary of the waves. Therefore, the resistance changes can be much larger in case of cellular bindings and their further interactions than in case of direct adsorption. In case of Figure 3A, the surface coverage of the CCRF-CEM controls is low as seen from the frequency shifts as well as from the microscopic images. This promotes the surface adsorption of the antibodies of the uncovered area of Au QCM electrode leading to higher frequency shift and relatively lower resistance change ($|\Delta f_0/\Delta R_1| \approx 66$ Hz Ω^{-1}). This situation is, however, cleared from the Figure 3B where we provided much longer time for the control cells to obtain a densely immobilized cells on the Au QCM surface, thereby reducing the chances of direct antibody adsorption on the Au QCM. Hence in this case, both the frequency and the resistance signals are correlated to each other ($|\Delta f_0/\Delta R_1| \approx 17$ Hz Ω^{-1}) and to the Raji Cells in Figure 3A ($|\Delta f_0/\Delta R_1| \approx 19$ Hz Ω^{-1}), although very small than the Raji Cells thereby showing a control response. This situation is depicted in the Scheme S1. This was the reason behind calculating the frequency resistance slope $|\Delta f_0/\Delta R_1|$ for the cell antibody interaction at the whole cell-capture phase in case of Figure 2 ($|\Delta f_0/\Delta R_1|_{\text{average}} \approx 24$ Hz Ω^{-1}). All these values are bigger than the threshold value i.e., 11.6 Hz Ω^{-1} for a 10 MHz crystal, to show a dominant mass effect. It means that the QCM responses can mainly be attributed to the mass effect. Figure S3 also shows that there was almost no aggregation among CCRF-CEM cells in growth medium in comparison to Raji cells which show strong aggregation under the microscope. So it was harder for these cells to be easily adhered on the electrode surface like Raji cells did, which means the number of captured CCRF-CEM cells was not large in a short time (two hours). As a result, the QCM signals induced by CCRF-CEM cells' attachment in Figure 3A1–A2 presented small changes. After a longer immobilization time (19 Hours) for control cells, three mAbs was introduced into the measuring chamber, respectively. Figure 3B1–B2 show that the three mAbs had no influence on the QCM responses. In addition, the investigations on the binding of the three mAbs on attachment cells were also conducted. As shown in Figure 3C1–C2, the capture of HUVEC-C cells led to the bigger frequency-changes than B cells and T cells. It indicates that more cellular adhesive molecules existed on the cell membrane of HUVEC-C cells and their immobilization on the RGD tripeptide modified electrode was easily achieved. After the addition of the three mAbs, no significant shift in the frequency and resistance curves occurred, retaining the trend of cell addition. This indicates the absence of antibody binding to the cell surface. These control experiments, all prove the specific binding of Rituximab to Raji cells based on the immune reaction between Rituximab and CD20.

The biointerface shows predominant mass effects which allow us to quantify the apparent binding constant between immobilized Raji Cells and Rituximab using QCM technique. The morphology of Raji cells in HBS in the absence and presence of Rituximab cultured at different time were observed, respectively, and the microscope photographs are shown in Figure S4. Raji cell is a spheroid at 0.5 h and 3 h. Sixteen hours later, some cells were in expansion but the cell morphology remained intact (Panels A1–A3), meaning that the cells could maintain integrality and some activity for a long time in the buffer without a supply of additional nutrition factors in growth medium. The intact cells can be still observed at 3 h after the addition of Rituximab and lots of cell fragments remained in the culture dishes after 16 h (Panels B1–B3). It reveals that Raji cells suffered lysis in the presence of Rituximab but this lysis was not a rapid process. Normally, the binding reaction is very fast, however, the mechanisms of action specifically proposed for the Rituximab suggest the opposite way.[41,42] In all these proposed mechanisms, there is no intracellular transport of the antibody involved and only the binding is required to trigger the process of lysis. Alduaij et

al[43] examined the role of lysosomes in monoclonal antibody-induced cell death by labeling Raji cells with the lysosome-specific dye, Lysotracker green, and found that Rituximab induced no changes in lysosomal volume and no collapse in a subpopulation of the cells after Raji cells were treated with Rituximab for 4 hours. Thus, the negative shifts of the frequency in the initial phases of the QCM experiments can only be assigned to the binding events. The QCM data at 3 hour after the addition of Rituximab, when Raji cell did not suffer lysis and still remained intact, were used. The QCM signal shifts in this period should be mainly derived from the binding between Rituximab and Raji cells rather than the cell lysis. Anderson et al has also shown that for high-affinity antibodies, the binding equilibrium cannot be established until at least few hours of interaction, and the calculations before that can result into false negative results.[44] Figure 4A depicts the Δf_0 signal-shifts of the cell-captured electrode vs. different concentrations of Rituximab. The changes of QCM signals increased with the Rituximab concentration. The $|(\Delta f_0)_n - (\Delta f_0)_0|$ is defined for the increased of Δf_0 signals, where $(\Delta f_0)_0$ and $(\Delta f_0)_n$ represents the frequency change induced by cell-capture in the absence and presence of Rituximab, respectively. The value of $|(\Delta f_0)_n - (\Delta f_0)_0|$ represents the net frequency responses derived from the Rituximab binding.

Based on the Sauerbrey equation:

$$\Delta f_0 = -k\Delta m \quad (3)$$

where the constant k is the value of $2f_{0g}^2/(\rho_q \mu_q)^{1/2}$. The frequency changes derived from the Rituximab binding to Raji cell modified electrode should be described as follows,

$$|(\Delta f_0)_n - (\Delta f_0)_0| = k\Delta m = k\Gamma \quad (4)$$

As we know, Langmuir adsorption equation can be expressed as,

$$\frac{c}{\Gamma} = \frac{c}{\Gamma_{max}} + \frac{1}{K \cdot \Gamma_{max}} \quad (5)$$

where c is the concentration of the added material, $\Gamma$is the adsorbed amount, Γ_{max} is the maximum adsorbed amount and K is Langmuir equilibrium constant, respectively.

A combination of Eq. (4) with Eq. (5) yields,

$$\frac{c}{|(\Delta f_0)_n - (\Delta f_0)_0|} = \frac{c}{\left|(\Delta f_0)_n - (\Delta f_0)\right|_{max}} + \frac{1}{K \cdot \left|(\Delta f_0)_n - (\Delta f_0)\right|_{max}} \quad (6)$$

Figure 4B shows that the value of $|(\Delta f_0)_n - (\Delta f_0)_0|$ was increased with increase of Rituximab concentration ($c_{Rituximab}$) but it gradually plateaued at higher $c_{Rituximab}$. The experimental data fits well to the Langmuir adsorption model. As shown in Figure 4C, $c_{Rituximab}/|(\Delta f_0)_n - (\Delta f_0)_0|$ exhibited a linear response with respect to $c_{Rituximab}$ over the range of the Rituximab concentration from 5 to 250 μg mL^{-1}. The regression equation was $c_{Rituximab}/|(\Delta f_0)_n - (\Delta f_0)_0| = 0.010\ c_{Rituximab} + 0.899$ with a high correlation coefficient of 0.996. The values of $|(\Delta f_0)_n - (\Delta f_0)_0|_{max}$ and the apparent binding constant K were calculated to be 100 Hz and 1.6×10^6 M^{-1}, respectively, based on the slope and intercept of the linear regression equation. The apparent binding constant value is smaller than the reported binding constant between Rituximab and CD20 antigen by Scatchard plotting based on radioimmunoassay, i.e., from 2.0×10^8 M^{-1} to 2.8×10^8 M^{-1}.[45,46] The decrease of the apparent binding constant between Rituximab and Raji cells up to two orders of magnitude can be attributed to the less surface

coverage of CD 20 on cell membranes as well as due to the involvement of multiple factors in the described experimental conditions. Thus, we have termed it as apparent binding constant. For our experimental design, the data still fit well into the simple Langmuir isotherm with good correlation coefficient, indicating that the probability of multiple interaction sites is low, and Rituximab binds with Raji cells in a single-layer manner. By this observation, the QCM technique is proven to be highly efficient to study these binding mechanisms between cell surface antigens and antibodies with great accuracy.

Characterization of CD20 on B cell membranes as a calcium channel

Bubien et al. reported an increased calcium conductance across the plasma membrane using cell lines transfected with CD20.[47] Some researchers have successfully reduced expression levels of CD20 in B-cell lines by employing antisense CD20 sequence and found a significantly decreased calcium entry across the plasma membrane.[1,48] These studies indicate that CD20 functions as an important calcium channel for regulating cell cycle progression and calcium homeostasis.

The real time monitoring of the binding of Rituximab to Raji cells in the presence of Ca^{2+} ion with different concentrations was performed and the results are shown in Figure 5A. One can find that the Δf_0 shifts induced by the Rituximab-binding to Raji cell modified electrode in the presence of Ca^{2+} ions were apparently bigger than those in the absence of Ca^{2+} ion. The Δf_0 changes increased with the augment of the Ca^{2+} concentration at the initial 6 hour after the addition of the Rituximab-Ca^{2+} combination. The involvement of increased intracellular Ca^{2+} levels in apoptosis has been reported in many cell types stimulated by different cell death-promoting factors.[49] Shan's experiments support the hypothesis that anti-CD20-induced apoptosis is mediated by increases in intracellular concentration of Ca^{2+}.[41] These investigations reveal that the intake of Ca^{2+} with high concentration resulted in high intracellular Ca^{2+} levels, which accelerated the cell apoptosis. It is reported that apoptotic cell death is typically paralleled by sustained activation of several channels, which fosters exit of K^+, Na^+, Cl^-, HCO_3^- and organic osmolytes.[50–53] Cellular loss of electrolytes and cytosolic acidification favor apoptosis. The efflux of these electrolytes from Raji cells balances the electrical neutrality in the cell system. However, a control experiment performed in the absence of Rituximab (the data shown in Figure S4) indicates that only Ca^{2+} ions cannot induce any fluctuations in the QCM plots. This means that the Rituximab-Ca^{2+} combination is required to induct changes in QCM frequency and motional resistance. This is quite logical too. First the ions are too small to significantly affect the QCM response. Second, the balance of influx and efflux is present to remove even the smallest effects. A recent study proves[50] that the influx of extracellular Ca^{2+} participates in and enhances the Rituximab controlled phenomena in the cell signaling mechanisms, thereby increasing the speed of drug binding activity and the resulting apoptosis. This has exactly happened in Figure 5, where the increasing levels of extracellular Ca^{2+} has caused the rapid binding of Rituximab. Therefore, in the first 3 hours, the QCM response increases with the increase of Ca^{2+} ion concentration. However, in the subsequent hours, the increased extracellular Ca^{2+} has caused the process of apoptosis to be more rapid, and the QCM plots quickly reached to the plateau for concentrations above 3 mM. In the first 3 hours, there is no significant lysis and the frequency decrease can be mostly attributed to antibody binding as explained in previous discussion. Both the cell adhesion to the QCM electrode and the binding of Rituximab to the CD-20 are dynamic process requiring long time scales thereby continuously increasing the QCM response (frequency being decreased and Δf_0 is increasing) which is proportional to the added Ca^{2+} ions. This is also seen in all the presented data in this paper where no plateau is observed even after as many as 20 hours. However, in the later parts of the curve (after 3 hours), the lysis of the cells start affecting the QCM response which is more and more significant with the increasing levels of Ca^{2+}

ions. In this case of significant cell lysis especially for concentrations above 3 mM, there will be no further changes in the binding as well as cell adhesion/detachment from the QCM surface leading to a plateau of response to be observed. At this stage, Δf_0 values are not increasing, rather a static condition is attained which has resulted in the plateaued QCM curves as in the case of plots (d–f) in figure 5.The microscope photographs of Raji cells in HBS in the presence of the Rituximab-Ca^{2+} combination cultured at different time are shown in Panels C1–C3 of Figure S5 which provide a confirmation of this phenomenon. One can find the intact Raji cells at 3 h after the addition of Rituximab in the presence of Ca^{2+} ions (Panel C2). It suggests that the lysis of Raji cells induced by the Rituximab-Ca^{2+} combination was not a rapid process. In a short time after addition of the Rituximab-Ca^{2+} combination (for example, 3 hours), Δf_0 responses should be mainly derived from the binding of Rituximab which increases with increase in the extracellular Ca^{2+}. It is also found that the cell fragments at 16 h after the stimulation with Rituximab in the presence of Ca^{2+} ions (Panel C3 of Figure S5) became smaller in size and in number than those in the absence of Ca^{2+} ions (Panel B3 of Figure S5). The result reveals that the cytotoxicity of the Rituximab-Ca^{2+} combination was more prominent than Rituximab alone and Ca^{2+} ions might accelerate the lysis process of Raji cells.

The Δf_0 data at the third hour after the addition of the Rituximab-Ca^{2+} combination in Figure 5A were investigated for analyzing the binding model between Rituximab-Ca^{2+} combination and the cells. Here, $|(\Delta f_0)_n - (\Delta f_0)_0|$ is defined for the increased extent of Δf_0 signals. But, unlike the definition in Figure 4B, $(\Delta f_0)_0$ and $(\Delta f_0)_n$ are the frequency changes induced by the binding of Rituximab to cells/RGD/PQCE in the absence and presence of Ca^{2+} ions, respectively. The value of $|(\Delta f_0)_n - (\Delta f_0)_0|$ represents the net frequency responses due to the influx of Ca^{2+} ions. The influx content of Ca^{2+} ions into the cells, $N_{Ca^{2+}(i)}$, could be obtained based on the $|(\Delta f_0)_n - (\Delta f_0)_0|$ value using Sauerbrey equation (Equation 1). It can be observed from Figure 5B that the $N_{Ca^{2+}(i)}$ value was enhanced with increasing c_{Ca}. The data were found to be fitted well to the Freundlich adsorption model. As shown in Figure 5C, log $N_{Ca^{2+}(i)}$ was linearly proportional to logc_{Ca} over the range of 0.15 to 10.0 mM. The regression equation was log $N_{Ca^{2+}(i)}$ = 0.223 logc_{Ca} + 2.38 with a high correlation coefficient of 0.995. The two constants, K and n, were calculated to be 6.0×10^{-9} and 4.5, respectively. In general, Freundlich adsorption model reveals multilayer adsorption phenomenon. The above experimental results indicate that Ca^{2+} ions could enter the cells continuously through CD20 instead of binding on cell surfaces in a single-layer manner.

It is reported that manganese ions can pass through calcium channels because they have a relatively low energy of hydration.[54] Figure S5 shows the real-time Δf_0 and ΔR_1 responses to the addition of Rituximab-Mn^{2+} combination to Raji cell modified electrode. Mn^{2+} with high concentration led to the obviously increased Δf_0 and ΔR_1 responses but all curves in Figure S5 do not show a plateau in the presence of Mn^{2+}, suggesting that Mn^{2+} ions could enter into cells through CD20 channel but did not contribute to the cell-lysis compared to the conditions with Ca^{2+} and Rituximab.

CONCLUSIONS

Antibody-mediated therapy has changed the paradigm for cancer treatment. A better understanding of antigen characteristics and the interactions between cell surface antigen and antibody therapeutics is crucial for the design of more effective therapies. In this work, we have studied the binding process between CD20 on B cells and therapeutic antibody drug Rituximab by multiple electrochemical methods (potentiometry, CV, EIS and QCM). No obvious interaction is found between the Trastuzumab and Bevacizumab to the immobilized Raji cells. The binding of Rituximab to T cells and endothelial cells was also not observed. All these results confirmed the specificity of the Rituximab to the Raji cell. The binding of

Rituximab to the Raji cell could decrease the electrochemical activity and stability of the cells indirectly supporting the cell lysis mechanisms. We have shown a systematic approach for using QCM technique to quantify the apparent binding constant between Raji cells and Rituximab. This binding constant was calculated to be 1.6×10^6 M^{-1} and a linear relationship between frequency shift and Rituximab concentration is obtained in the range of 5–250 μg mL^{-1} of Rituximab. The further increased QCM responses were found by the Rituximab addition in the presence of Ca^{2+} ions and high-concentration Mn^{2+} ions, supporting the function of CD20 as a calcium ion channel. Microscopic inspection proved that Ca^{2+} ions could promote the Rituximab binding and cell lysis induced by Rituximab. In summary, this work presents a quantitative label free method based on QCM transducer to characterize cell surface antigen and antibody interactions, which can be applied to obtain in depth understanding of the binding event to facilitate the comprehension of the mechanisms of resistance to antibody based therapy.

Supplementary Material

Refer to Web version on PubMed Central for supplementary material.

Acknowledgments

X Zeng likes to thank NIH R21 grant (R21EB006495) and OU Beaumont interdisciplinary support.

REFERENCES

1. Deans JP, Li H, Polyak MJ. Immunology. 2002; 107:176. [PubMed: 12383196]
2. Nadler LM, Ritz J, Hardy R, Pesando JM, Schlossman SF, Stashenko P. The Journal of clinical investigation. 1981; 67:134. [PubMed: 6969730]
3. Riley JK, Sliwkowski MX. Seminars in oncology. 2000; 27:17. [PubMed: 11225995]
4. Maloney DG, Grillo-Lóez AJ, White CA, Bodkin D, Schilder RJ, Neidhart JA, Janakiraman N, Foon KA, Liles T-M, Dallaire BK, Wey K, Royston I, Davis T, Levy R. Blood. 1997; 90:2188. [PubMed: 9310469]
5. Leget GA, Czuczman MS. Current Opinion in Oncology. 1998; 10:548. [PubMed: 9818234]
6. Boye J, Elter T, Engert A. Annals of Oncology. 2003; 14:520. [PubMed: 12649096]
7. Check E. Nature. 2004; 428:786. [PubMed: 15103338]
8. Edwards JCW, Szczepański L, Szechiński J, Filipowicz-Sosnowska A, Emery P, Close DR, Stevens RM, Shaw T. New England Journal of Medicine. 2004; 350:2572. [PubMed: 15201414]
9. McLaughlin P, Grillo-Lóez AJ, Link BK, Levy R, Czuczman MS, Williams ME, Heyman MR, Bence-Bruckler I, White CA, Cabanillas F, Jain V, Ho AD, Lister J, Wey K, Shen D, Dallaire BK. J. Clin. Oncol. 1998; 16:2825. [PubMed: 9704735]
10. Davis TA, Grillo-Lóez AJ, White CA, McLaughlin P, Czuczman MS, Link BK, Maloney DG, Weaver RL, Rosenberg J, Levy R. J. Clin. Oncol. 2000; 18:3135. [PubMed: 10963642]
11. Bingaman MG, Basu GD, Golding TC, Chong SK, Lassen AJ, Kindt TJ, Lipinski CA. Anti-Cancer Drugs. 2010; 21:532. [PubMed: 20216307]
12. Johnson NA, Boyle M, Bashashati A, Leach S, Brooks-Wilson A, Sehn LH, Chhanabhai M, Brinkman RR, Connors JM, Weng AP, Gascoyne RD. Blood. 2009; 113:3773. [PubMed: 19029441]
13. Almasri NM, Duque RE, Iturraspe J, Everett E, Braylan RC. American Journal of Hematology. 1992; 40:259. [PubMed: 1380203]
14. Tzankov A, Krugmann J, Fend F, Fischhofer M, Greil R, Dirnhofer S. Clinical Cancer Research. 2003; 9:1381. [PubMed: 12684408]
15. Lenkei R, Gratama JW, Rothe G, Schmitz G, D'Hautcourt JL, Årekrans A, Mandy F, Marti G. Cytometry. 1998; 33:188. [PubMed: 9773879]
16. Marx KA. Biomacromolecules. 2003; 4:1099. [PubMed: 12959572]

17. Cheng CI, Chang YP, Chu YH. Chemical Society Reviews. 2012; 41:1947. [PubMed: 22158962]
18. Sauerbrey G. Z. Physik. 1959; 155:206.
19. Kanazawa KK, Gordon JG. Analytical Chemistry. 1985; 57:1770.
20. Martin SJ, Granstaff VE, Frye GC. Analytical Chemistry. 1991; 63:2272.
21. Granstaff VE, Martin SJ. Journal of Applied Physics. 1994; 75:1319.
22. Shang Y, Mernaugh R, Zeng X. Analytical Chemistry. 2012; 84:8164. [PubMed: 22934911]
23. Shang Y, Singh PR, Chisti MM, Mernaugh R, Zeng X. Analytical Chemistry. 2011; 83:8928. [PubMed: 21961885]
24. Shen Z, Mernaugh RL, Yan H, Yu L, Zhang Y, Zeng X. Analytical Chemistry. 2005; 77:6834. [PubMed: 16255580]
25. Shen Z, Stryker GA, Mernaugh RL, Yu L, Yan H, Zeng X. Analytical Chemistry. 2005; 77:797. [PubMed: 15679346]
26. Shen Z, Yan H, Parl FF, Mernaugh RL, Zeng X. Analytical Chemistry. 2007; 79:1283. [PubMed: 17297925]
27. Shen Z, Yan H, Zhang Y, Mernaugh RL, Zeng X. Analytical Chemistry. 2008; 80:1910. [PubMed: 18290668]
28. Yan H, Shen Z, Mernaugh R, Zeng X. Analytical Chemistry. 2011; 83:625. [PubMed: 21230001]
29. Arap W, Pasqualini R, Ruoslahti E. Science. 1998; 279:377. [PubMed: 9430587]
30. Ruoslahti E. Annual Review of Cell and Developmental Biology. 1996; 12:697.
31. Chandrasekera PC, Kargacin ME, Deans JP, Lytton J. American Journal of Physiology - Cell Physiology. 2009; 296:C1105. [PubMed: 19225163]
32. Hao C, Ding L, Zhang X, Ju H. Analytical Chemistry. 2007; 79:4442. [PubMed: 17492835]
33. Ding L, Hao C, Xue Y, Ju H. Biomacromolecules. 2007; 8:1341. [PubMed: 17375952]
34. Hao C, Yan F, Ding L, Xue Y, Ju H. Electrochemistry Communications. 2007; 9:1359.
35. Chen J, Du D, Yan F, Ju HX, Lian HZ. Chemistry – A European Journal. 2005; 11:1467.
36. Yan F, Chen J, Ju H. Electrochemistry Communications. 2007; 9:293.
37. Wang J, Zhou F. Journal of Electroanalytical Chemistry. 2002; 537:95.
38. Du D, Liu S, Chen J, Ju H, Lian H, Li J. Biomaterials. 2005; 26:6487. [PubMed: 15951013]
39. Cartron G, Watier H, Golay J, Solal-Celigny P. Blood. 2004; 104:2635. [PubMed: 15226177]
40. Xie Q, Wang J, Zhou A, Zhang Y, Liu H, Xu Z, Yuan Y, Deng M, Yao S. Analytical Chemistry. 1999; 71:4649.
41. Shan D, Ledbetter JA, Press OW. Cancer Immunol Immunother. 2000; 48:673. [PubMed: 10752475]
42. Tedder TF, Engel P. Immunology Today. 1994; 15:450. [PubMed: 7524522]
43. Alduaij W, Ivanov A, Honeychurch J, Cheadle EJ, Potluri S, Lim SH, Shimada K, Chan CH, Tutt A, Beers SA, Glennie MJ, Cragg MS, Illidge TM. Blood. 2011; 117:4519. [PubMed: 21378274]
44. Björkelund H, Gedda L, Andersson K. Journal of Molecular Recognition. 2011; 24:81. [PubMed: 21194119]
45. Reff M, Carner K, Chambers K, Chinn P, Leonard J, Raab R, Newman R, Hanna N, Anderson D. Blood. 1994; 83:435. [PubMed: 7506951]
46. Du J, Wang H, Zhong C, Peng B, Zhang M, Li B, Huo S, Guo Y, Ding J. The Journal of biological chemistry. 2007; 282:15073. [PubMed: 17395584]
47. Bubien JK, Zhou LJ, Bell PD, Frizzell RA, Tedder TF. The Journal of Cell Biology. 1993; 121:1121. [PubMed: 7684739]
48. Li H, Ayer LM, Lytton J, Deans JP. Journal of Biological Chemistry. 2003; 278:42427. [PubMed: 12920111]
49. Dowd DR. Advances in second messenger and phosphoprotein research. 1995; 30:255. [PubMed: 7695993]
50. Fengling M, Qingxiang G, Lijia Z, Wei Z. Toxicology letters. 2012; 209:221. [PubMed: 22245670]

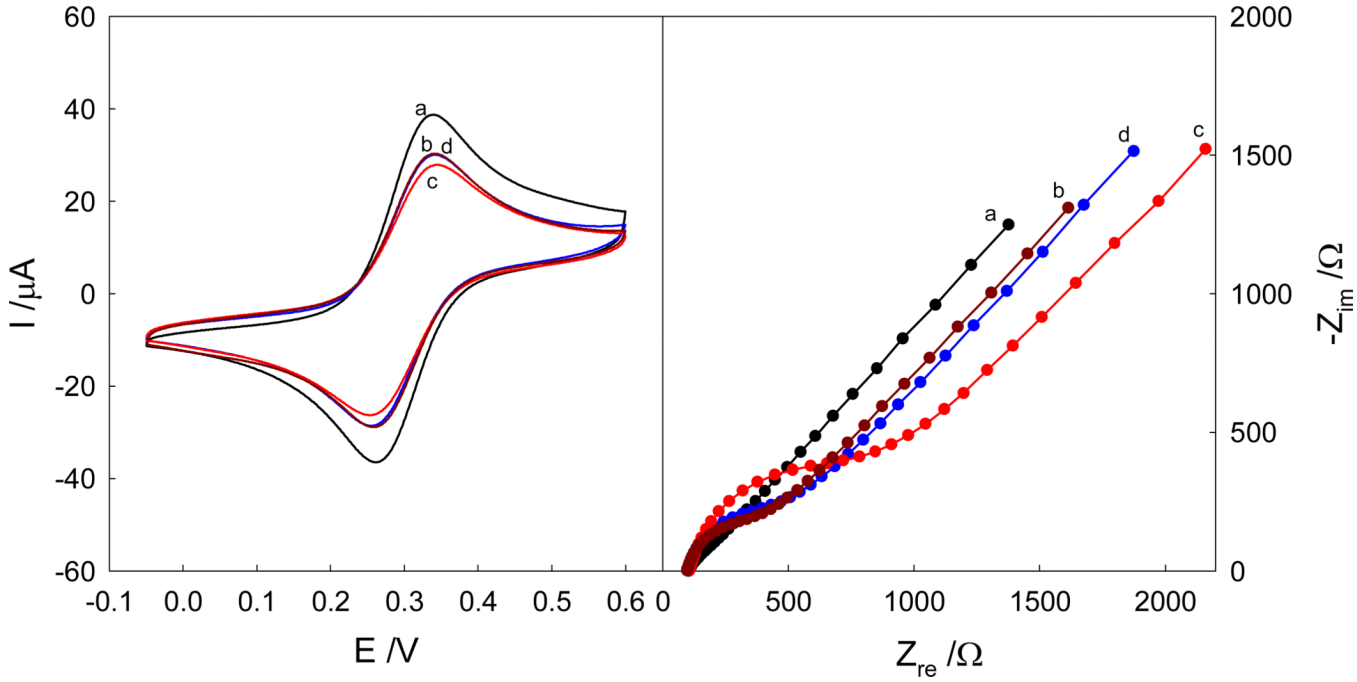

Figure 1.

Cyclic voltammograms (A) and electrochemical impedance spectra (B) of Au electrode (a), Au/RGD (b), Au/RGD/cells before (c) and after (d) the 16-h treatment of 150 μg mL^{-1} Rituximab in a pH 7.4 PBS containing 1 mM $K_3Fe(CN)^6$, 1 mM $K_4Fe(CN)^6$, and 0.2 M KNO_3. (A) Scan rate: 50 mV s^{-1}; (B) AC frequency range: 100 kHz ~ 5 mHz, amplitude: 10 mV, DC bias: 0.30 V, reference electrode: saturated Ag/AgCl.

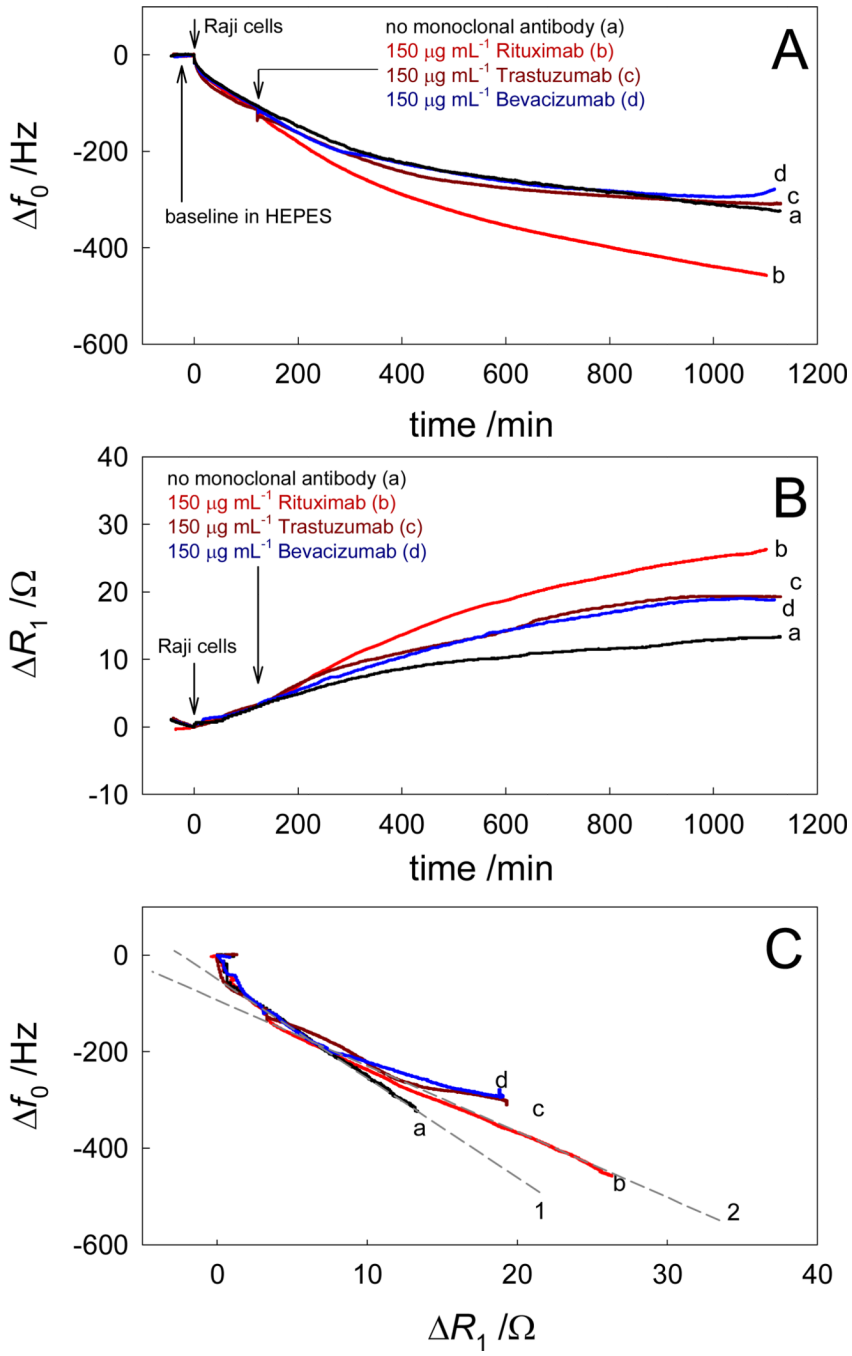

Figure 2.

Real-time Δf_0 (A) and ΔR_1 (B) responses to the successive addition of 5×10^4 Raji cells and different monoclonal antibodies (2 h later) as well as the relationships of Δf_0 *vs*. ΔR_1 (C).

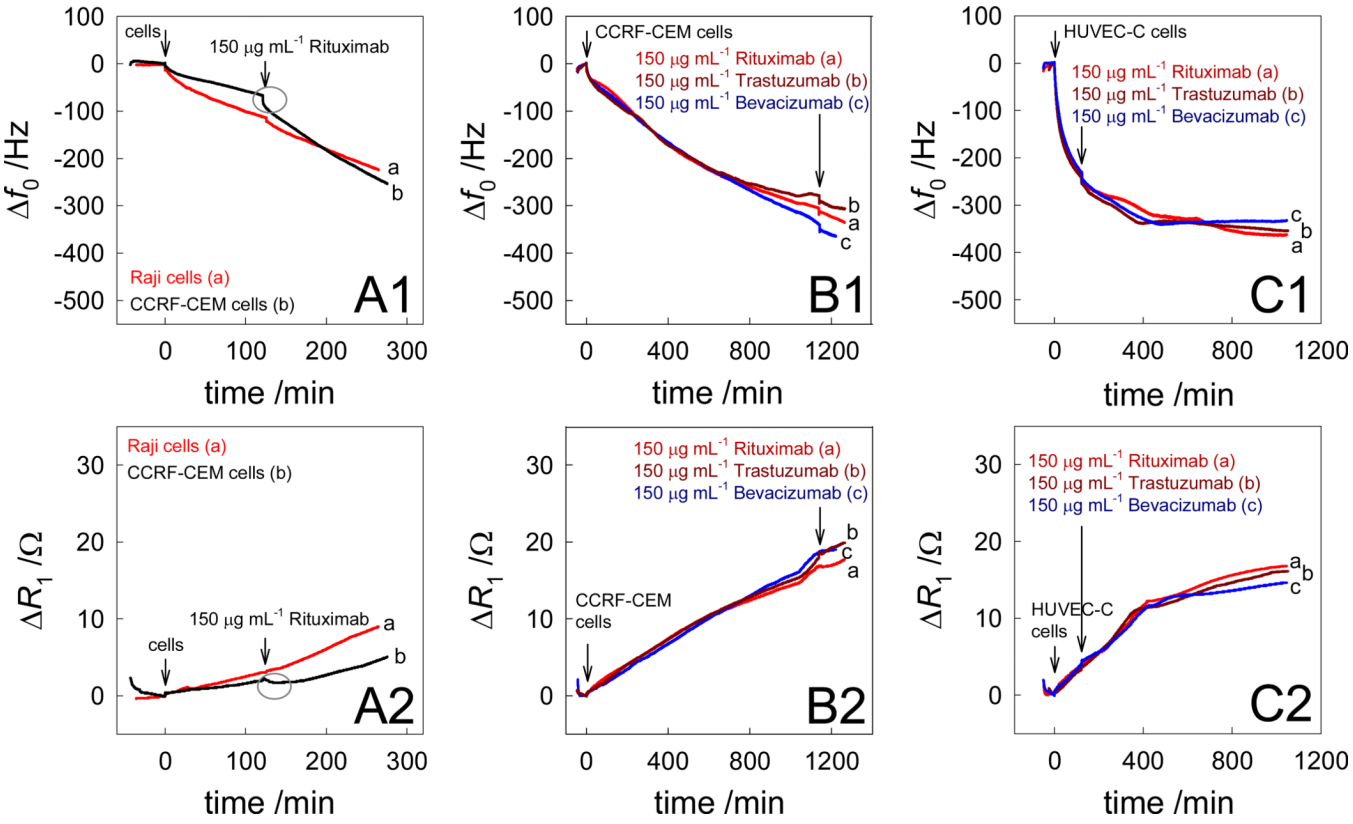

Figure 3.

(A) Real-time Δf_0 (A1) and ΔR_1 (A2) responses to the successive addition of 5×10^4 suspension cells and Rituximab (2 h later). (B) Real-time Δf_0 (B1) and ΔR_1 (B2) responses to the successive addition of 5×10^4 CCRF-CEM cells and different monoclonal antibodies (19 h later). (C) Real-time Δf_0 (C1) and ΔR_1 (C2) responses to the successive addition of 1.8×10^4 HUVEC-C cells and different monoclonal antibodies (2 h later).

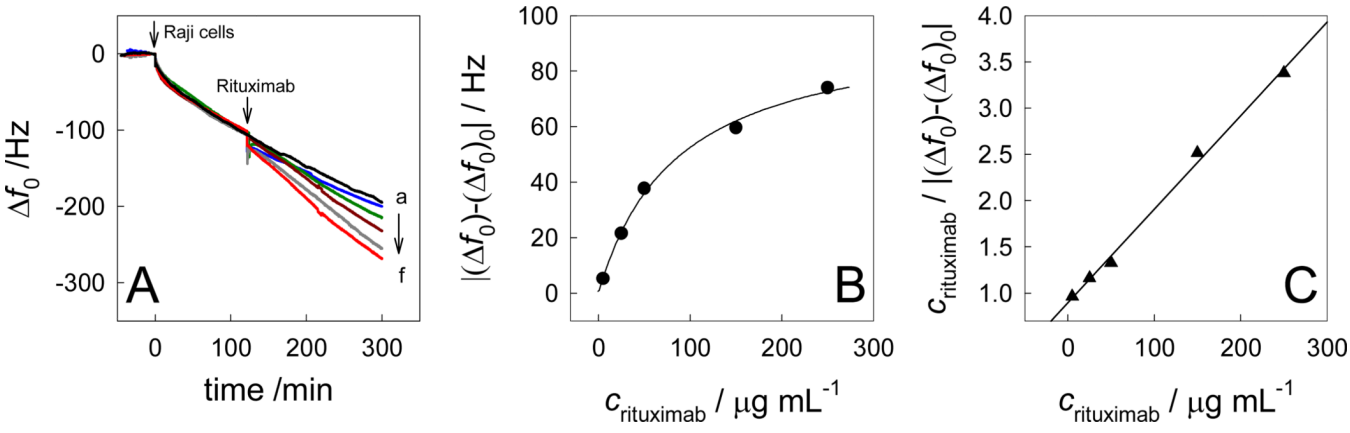

Figure 4.

(A) Real-time Δf_0 responses to the successive addition of 5×10^4 Raji cells and Rituximab with different concentrations (2 h later). The concentrations of Rituximab: 0, 5, 25, 50, 150 and 250 μg mL^{-1} from a to f. (B) Plot of $|(\Delta f_0)_n-(\Delta f_0)_0|$ vs. $c_{Rituximab}$. (C) Plot of $c_{Rituximab}/|(\Delta f_0)_n-(\Delta f_0)_0|$ vs. $c_{Rituximab}$.

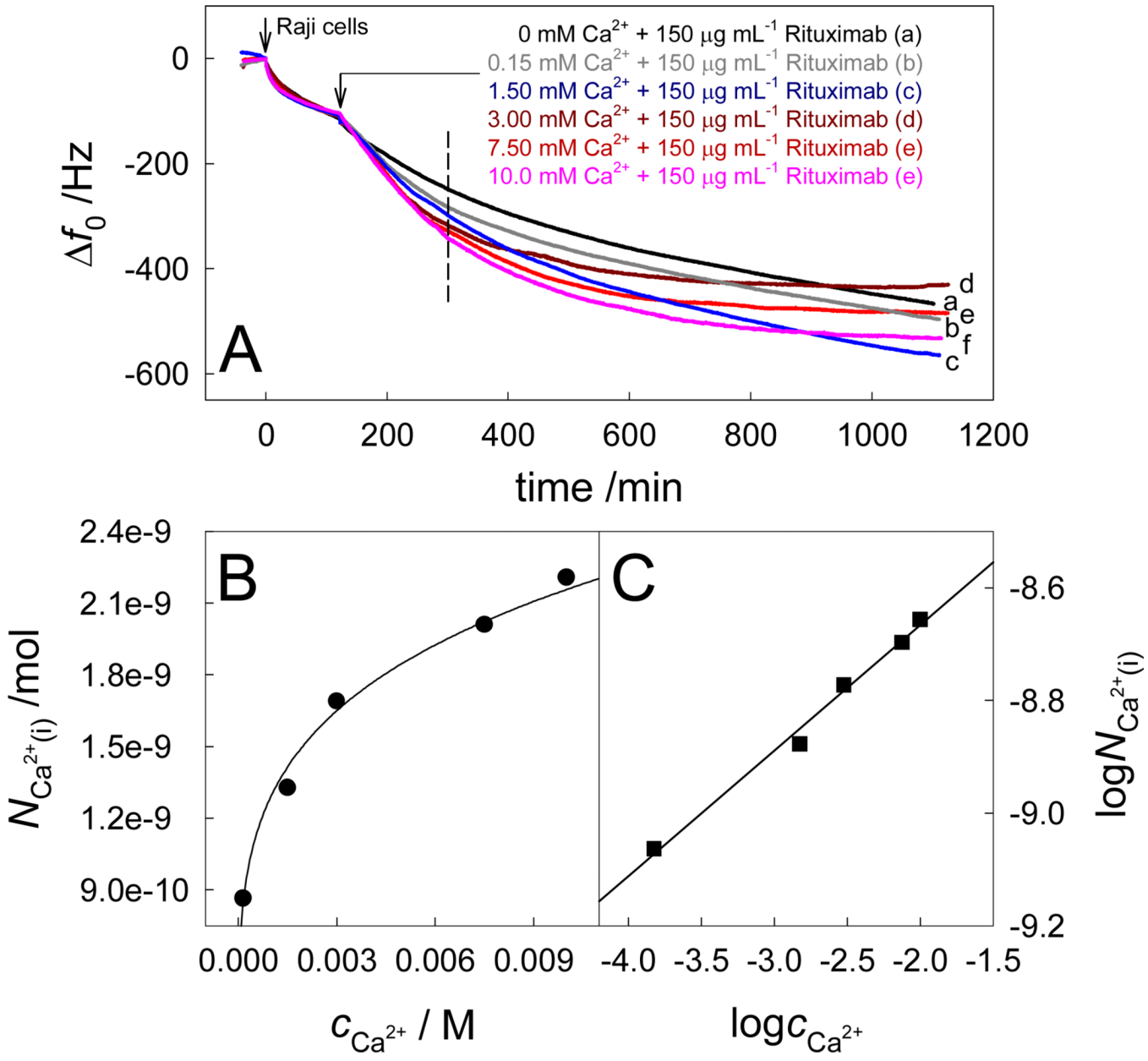

Figure 5.

(A) Real-time Δf_0 responses to the successive addition of 5×10^4 Raji cells and the Rituximab-Ca^{2+} combination with different Ca^{2+}-concentrations (2 h later). (B) Plot of $N_{Ca^{2+}(i)}$ vs c_{Ca}. (C) Plot of log $N_{Ca^{2+}(i)}$ vs logc_{Ca}

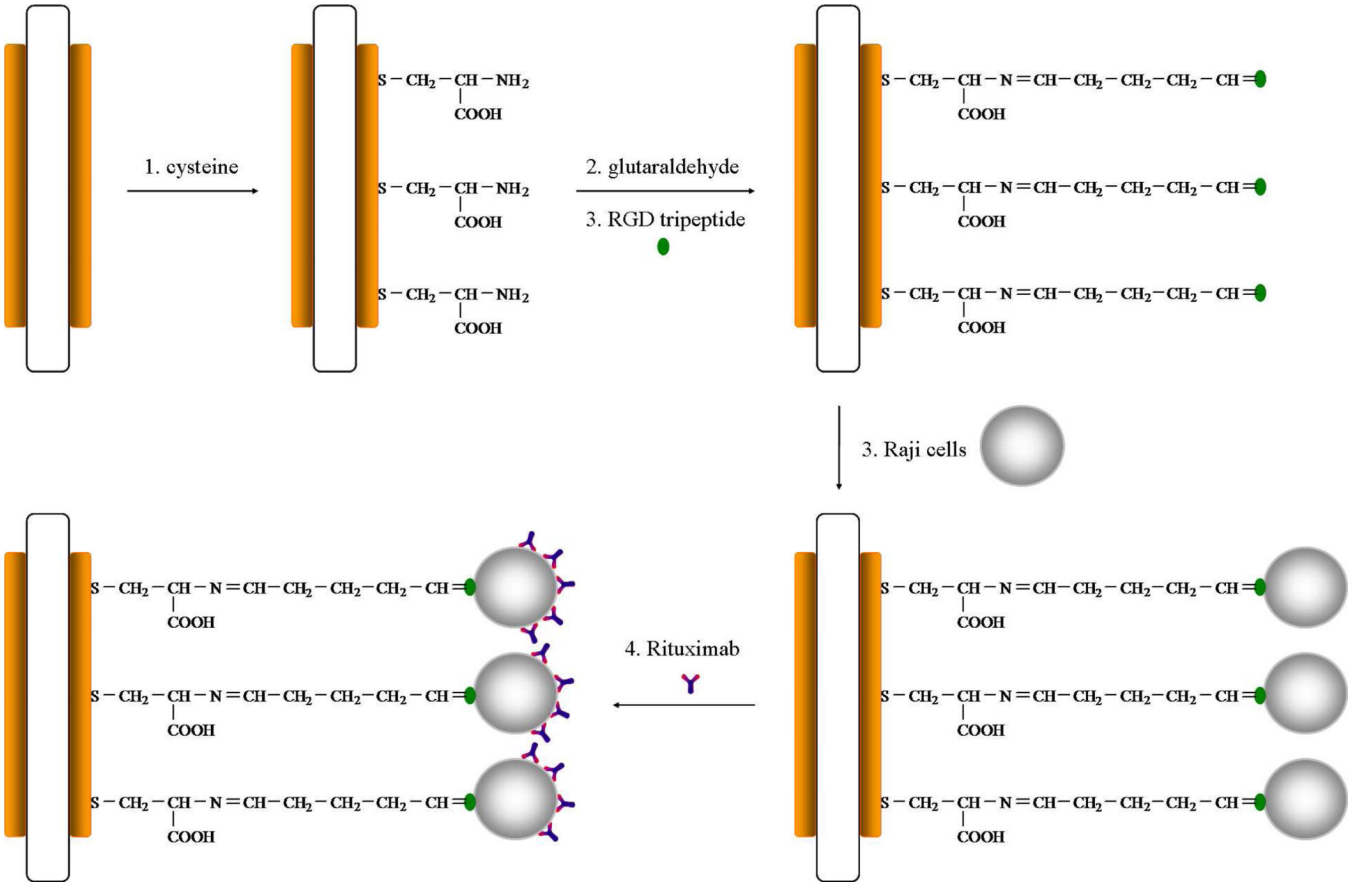

Scheme 1.
Binding of Rituximab on the B-cell captured QCM gold electrode.